Journal of Materials Chemistry C

ROYAL SOCIETY OF CHEMISTRY

PERSPECTIVE

View Article Online
View Journal | View Issue

Cite this: J. Mater. Chem. C, 2022, 10, 13717

Beyond electrical conductance: progress and prospects in single-molecule junctions

Chaolong Tang,†[a] Ridwan Tobi Ayinla†[b] and Kun Wang*[ab]

Received 22nd March 2022,
Accepted 1st June 2022

DOI: 10.1039/d2tc01155g

rsc.li/materials-c

The idea of using individual molecules as conducting wires, regulators, and interconnects for charges in electronic circuitry has catalyzed the vibrant development of the field of single-molecule electronics. The ability to reliably and repeatedly construct single-molecule junctions (SMJs) has enabled the study of charge transport through a broad spectrum of individual molecules. Over the past decade, the capability of the SMJ platform has been greatly expanded thanks to the development of new experimental techniques and the integration of knowledge and methodologies from other disciplines. New opportunities beyond electrical conductance have emerged at the atomic and molecular scale. It has been demonstrated in many recent studies that the SMJ can now serve as a powerful and versatile tool to address critical physical and chemical questions that are otherwise inaccessible. This perspective focuses on the new capabilities and functionalities of the SMJ beyond conductance measurements and how they have enabled the investigation of crucial single-molecule processes and advanced our understanding beyond molecular electronics.

1. Introduction

In 1974, Aviram and Ratner first introduced the visionary idea that a single molecule can be integrated into electronic circuits and act as a functional device, which laid out an exciting blueprint for scaling down electronic devices to the molecular scale.[1] Since then, there has been exponential growth in the experimental and theoretical efforts by researchers to understand charge transport through individual molecules.[2–8] The possibility of probing and manipulating the intrinsic properties of molecules at the atomic and molecular scale is credited to the development of revolutionary experimental techniques that enable the construction of single-molecule junctions (SMJs), including scanning tunnelling microscope break junctions (STMBJ),[9] mechanically controlled break junctions (MCBJ),[10] the conductive atomic force microscopy (CAFM) method,[11] electromigration break junctions (EBJ),[12] and graphene–molecule–graphene (GMG) SMJs.[13] Didactically, these robust and powerful techniques involve measuring the charge transport properties (in most cases the electrical conductance) of a single molecule trapped between two conductive electrodes.[2,14] Over the past two decades, the success of the SMJ techniques has led to impressive progress in understanding how the structure of a single molecule determines its electrical conductance. Insights from these studies have inspired the design and fabrication of single-molecule rectifiers,[15–23] transistors,[24–28] and switches.[29–35]

As the field proceeds to explore more complex molecular structures and junction architectures and interfaces with other disciplines, researchers have started to fully unveil the hidden potential of SMJs in serving as a fertile single-molecule platform for probing physical, chemical, and biological phenomena beyond electrical conductance.[36–39] It is striking to see that some elegant experimental studies in recent years have demonstrated the possibility to drive and monitor chemical reactions,[40,41] harness the interference of electron waves,[42] achieve heat-to-electricity energy conversion,[43] manipulate electron spins,[44] and reveal detailed structural variations[45] at the single-molecule level. Noticeably, these intriguing physical and chemical effects are far beyond the original vision of using single molecules just as electronic components. This paradigm shift has clearly injected new momentum for expanding the frontiers of single-molecule studies.

In 2013, Aradhya *et al.* published a forward-looking review on some of the central ideas beyond simple charge transport in SMJs.[37] After a decade, many new opportunities and directions have emerged. In this perspective, we aim to provide insights into recent breakthroughs in probing and understanding single-molecule phenomena beyond conductance measurements using the SMJ platform (Fig. 1). We first present the progress in catalyzing and monitoring chemical reactions at the single-molecule level. We then discuss the investigation of quantum interference (QI), heat transport, and thermoelectric energy

[a] Department of Physics and Astronomy, Mississippi State University, Mississippi State, MS 39762, USA. E-mail: kw2504@msstate.edu
[b] Department of Chemistry, Mississippi State University, Mississippi State, MS 39762, USA
† These authors contributed equally to this work.

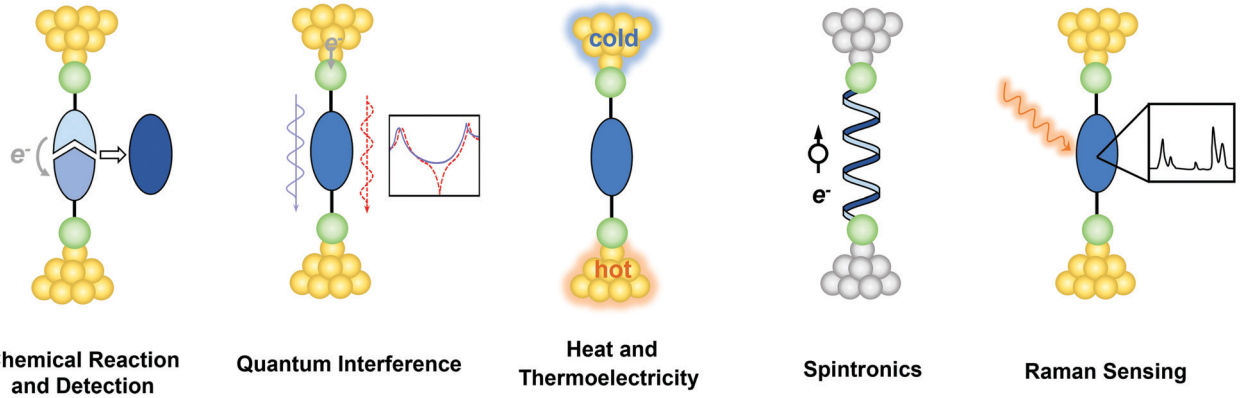

Fig. 1 Schematic illustration of single-molecule physical and chemical phenomena beyond electrical conductance explored in the SMJ.

conversation at the molecular scale. In what follows, we survey the recent efforts in probing spintronics in SMJs with particular attention to the chiral induced spin selectivity (CISS) effect and spin transport. Lastly, we introduce promising detection schemes combining SMJ with Raman spectroscopy to reveal the structural information on the molecules. We conclude by offering our perspective on the broad impact of the SMJ technique on many related research areas. We note that the scope of this article focuses on underlining the progress and potential of these emerging directions rather than offering a thorough review of each of the topics.

2. Driving and monitoring chemical reactions

One of the most promising and practical advantages of the SMJ is its ability to drive and monitor a chemical reaction at the single-molecule level, which offers an unambiguous route to understand, analyze, and manipulate the kinetics and dynamics of a chemical reaction in real-time. SMJ also provides the unique opportunity to examine the impact of external stimuli, such as electric field, electron injection, pH, and light. A variety of chemical reactions, including those that are not achievable in bulk measurements, have been reported in recent studies. Upon establishing a mechanically stable junction, researchers can now rely on the electrical current of an SMJ to detect detailed events related to stepwise reaction transformations and further capture a comprehensive single-molecule picture of the reaction dynamics. In this section, we provide a brief survey of representative reports on electric field-induced reactions and electron catalyzed chemical reactions using BJ techniques, and the detection of reaction dynamics using the GMG-SMJ technique. For a more detailed overview of this topic, we refer readers to relevant reviews.[40,46,47]

2.1 Electric field-assisted reactions and catalysis

Aligning the external electric field (EEF) in the forward reaction coordinate favors electronic rearrangement of interacting reactant species to form new products and reversing the electric field orientation will simply hinder the product formation.[48] This effect is also referred to as electrostatic catalysis. Specifically, EEF has been reported to have different effects in distinct reaction environments. For example, EEF oriented in the forward reaction axis speeds up the reaction rate, enhances elicit mechanistic crossing, allows spin state selectivity, and controls regioselectivity.[49,50] One of the commonly used reactions to synthesize fine chemicals and complex products is the Diel–Alder reaction. This reaction involves electron transfer from electronically symmetric dienophile and conjugated diene that results in the creation of a C–C bond.[51] Theoretical results of Meir *et al.* suggested that an electric field oriented in the direction of electron flow decreases the reaction barrier in the Diel–Alder reaction.[48] Although the use of EEF to control isomerization and selectivity has been long established in theories, more challenges prevail with the quest to orient EEF with the reaction coordinate of the molecule. In addition, EEF-driven reactions involving redox-inactive molecules remained impossible until very recently.

An STM setup offers a viable route to overcome the EEF alignment issue because the molecule between the STM tip and substrate is continuously exposed to a highly oriented local electric field. In 2016, using an STM-based technique, Aragonès *et al*.[52] successfully demonstrated the first EEF mediated Diel–Alder reaction in an SMJ containing redox-inactive molecules. In their experiments, the two reacting species (tethered furan derivative diene and rigid norbornylogous bridge dienophile) were attached to the gold STM tip and substrate, respectively. They applied a potential difference between the electrodes bearing the reacting species to create the oriented external electric field (OEEF) and approached the tip to the bottom substrate to bring the two reactants in proximity. A schematic of the experimental setup is shown in Fig. 2a. Stages 1, 2, and 3 illustrate a real-time current before, during, and after junction formation (or the completion of the reaction), respectively (Fig. 2b). Their work explicitly proved that C–C bond formation in non-polar reactions could be catalyzed using an oriented electric field in SMJs.

In 2021, Yang *et al.* attempted to elucidate the reaction dynamics of the Diel–Alder reaction using their characteristic GMG-SMJ[13] in the presence of the electric field.[53] They systematically investigated the real-time structural changes by applying a

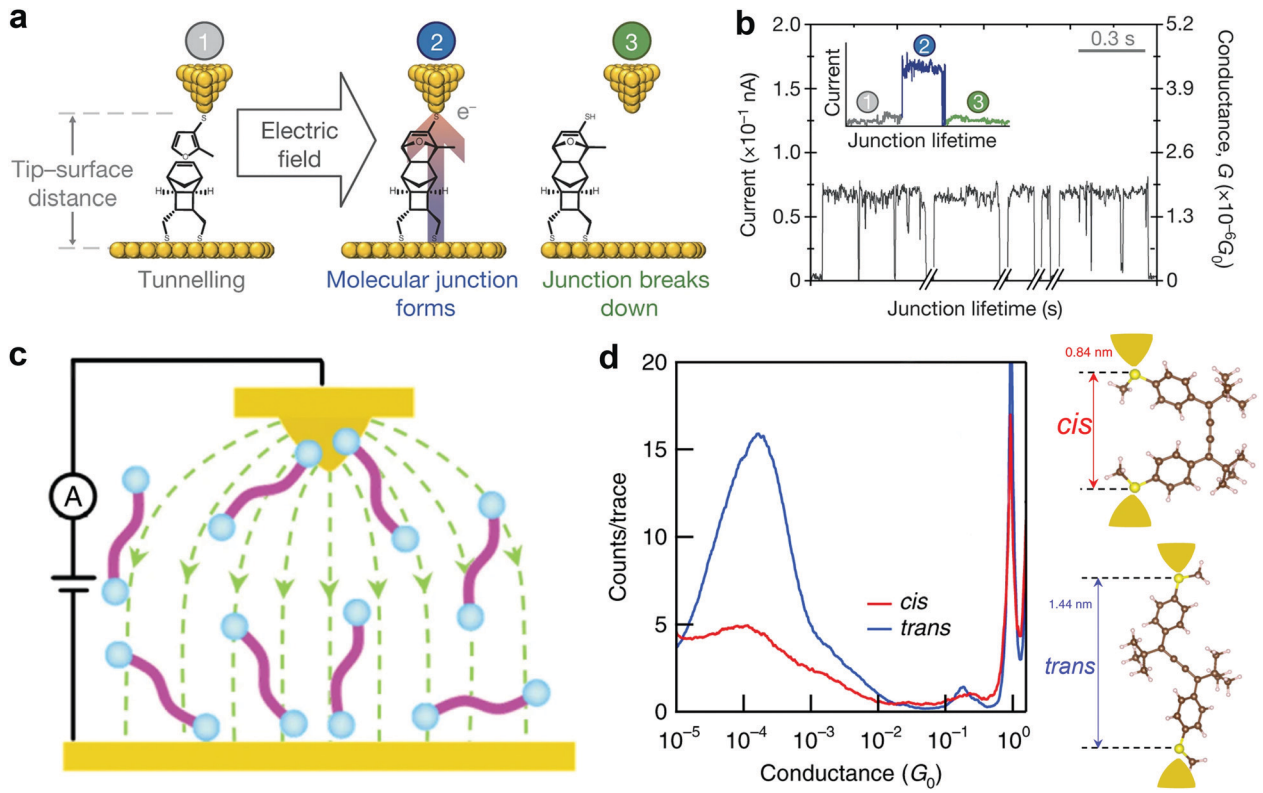

Fig. 2 (a) Stages featured during the blinking of the junction. (b) Real-time data capture of blinking events. The time breaks in the *x* axis are about 2 min. The inset shows the STM current response before (1), during (2) and after (3) the formation of a single blink (junction). Figures reproduced with permission from ref. 52. Copyright 2016, Springer Nature. (c) A schematic of the STM setup and the electric field distribution between the STM tip and substrate (green line). (d) Logarithm-binned 1D histograms for *cis* (red) and *trans* (blue) measured in tetradecane at a 0.1 V bias created by compiling 5000 and 9000 conductance traces, respectively. Inset: Density functional theory (DFT)-optimized structures of *cis* and *trans* isomers. Figures reproduced with permission from ref. 55. Copyright 2019, Springer Nature.

constant potential difference between the source and the drain graphene electrode while monitoring the electrical current of the junction at 393 K. Six random and stable current switches in the reaction of single furan with maleimide were observed, corresponding to six different stable structures. They employed temperature-dependent measurement and liquid phase concentration to determine the structural species corresponding to each current profile. Their experiment also showed that at low concentrations, low conductance states are more prominent. At low temperature, the ratio of second and third conductance states is proportional to the furan concentration. This signature implies the formation of the endo (more probable) and exo configurations with charge-transfer complexes. They concluded that the energy barrier of stepwise and concerted reactions is significantly lowered with strong EEF.

In another report, Huang *et al.* experimentally and theoretically designed a two-step cascade reaction involving the Diel–Alder reaction followed by an aromatization reaction.[54] They used OEEF to catalyze and induce selectivity using an MCBJ setup at room temperature. They concluded that the OEEF is orthogonal and non-orthogonal to the Diel–Alder addition and the aromatization reaction, respectively. Their result also affirmed the unique selective and catalytic role of the oriented electric field in a chemical reaction at the single-molecule level.

Notably, Zang *et al.* recently used an electric field to direct and catalyze isomerization reactions using the STMBJ technique in solution (Fig. 2c).[55] They showed an electric field-assisted *cis* to *trans* isomerization of cumulene derivatives. The *cis* conformation was verified by observing a lower conductance and a shorter conductance plateau length (Fig. 2d). An increase in the conductance and plateau length corresponding to the switch from the *cis* to *trans* conformation (Fig. 2d) was clearly observed. They also noticed the inhibition of the *trans* to *cis* switching in the presence of an electric field, suggesting that an electric field induced the selectivity of the *trans* conformation. Several other relevant electric field-driven reactions have been reported in the literature, and for more details, we refer readers to ref. 50.

2.2 Electron-catalyzed chemical reactions

The injection of an electron (reduction) into a trapped molecule in the SMJ induces pressure on the already existing electron and consequently leads to electronic rearrangement of the molecule. Real-time monitoring of the electronic rearrangements has shown that electrons can trigger a conformational switch, dehydrogenate, and switch bond states in a molecule at the single-molecule level.[56–58]

Chen *et al.* observed that linear and cyclic saturated 1,2-di(4-pyridinium)ethane (DPA^{2+}) showed a similar conductance

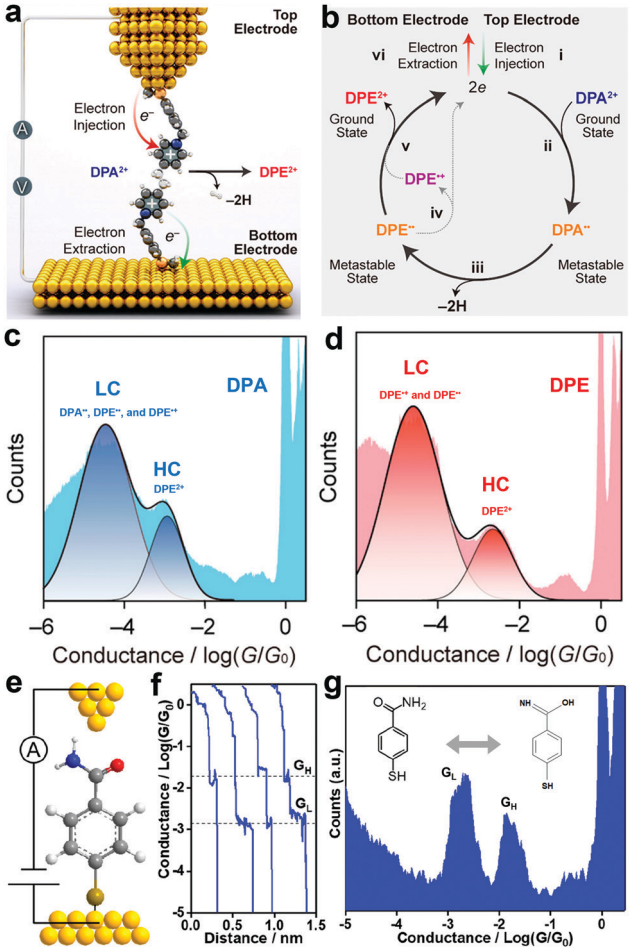

Fig. 3 (a) Schematic representation of electron-catalyzed DPA^{2+} to DPE^{2+} dehydrogenation in an STM junction. (b) A plausible mechanism for the electron catalyzed DPA^{2+}-to-DPE^{2+} dehydrogenation. (c and d) 1D conductance-displacement histograms of DPA^{2+}-to-DPE^{2+}, respectively. Figures reproduced with permission from ref. 57. Copyright 2021, American Chemical Society. (e) Schematic illustration of the STMBJ measurement of an SMJ containing an MBAm molecule. (f) Typical conductance decay traces were recorded in STMBJ measurements at 0.1 V bias in DI water. (g) Logarithm-binned conductance histogram for MBAm, showing two distinct conductance peaks at $10^{-2.72}$ and $10^{-1.78}$ G_0, respectively. Figures reproduced with permission from ref. 58. Copyright 2021, American Chemical Society.

profile with linear and cyclic unsaturated 1,2 di(4-pyridinium)-ethene (DPE^{2+}) (Fig. 3c and d).[56] The two pyridinium rings in DPA^{2+} are not on the same plane and are separated by saturated $-CH_2CH_2-$ which breaks the continuity in conjugation. Conversely, the pyridinium rings in DPE^{2+} enjoy unsaturated –CH═CH– separation, allowing an extended, continuous, and more efficient π conjugation. By convention, the DPA^{2+} is expected to have a lower conductance value relative to the DPE^{2+}. Their observation was counterintuitive, so they investigated the reaction mechanism of linear and cyclic molecules with DPA^{2+} and DPE^{2+} backbones in solution using an STMBJ setup (Fig. 3a and b).[57] They reported an electron catalyzed dehydrogenation of DPA^{2+} to DPE^{2+}. Step (i) depicts the injection of two electrons from the top electrode into the stable ground state DPA^{2+}, which resulted in the formation of a metastable DPA diradical step (ii). The saturated radical then undergoes dehydrogenation, which leads to the formation of a metastable DPE diradical step (iii). The reaction loop is completed by the ejection of two electrons from the metastable unsaturated diradical into the bottom electrode step (iv and v). Their report demonstrated that the injected electrons could effectively catalyze dehydrogenation reactions.

Huang *et al.* studied chemical bond switching in amides in an STMBJ (Fig. 3e).[58] Conventionally, amides can form different iminol tautomers. Specifically, the amide is understood to exist and have a resonance structure with a partial double bond between nitrogen and carbon. The resonance in the C–N bond is particularly important because it determines the planarity and stabilization of amide. In their study, they trapped 4-mercaptobenzamide (MBAm) between the nanogap of two gold electrodes to monitor the real-time conductance profile (Fig. 3f). They were able to experimentally show the transition between single and double bonds of amide, which have two distinct conductance states. The bimodal conductance feature comprises low (G_L) and high (G_H) conductance unique to the transition of the stable C–N and the less stable C═N isomers of amide (Fig. 3g). The high conductance of the C═N isomer is consistent with the more delocalized nature of the π-electron in the double bond. Their results provided detailed insights about the planarity, stability, and reactivity of amide.

2.3 Unveiling the dynamics of chemical reactions

Understanding the dynamics and trajectories of chemical reactions is central to synthetic chemistry. Therefore, the search for a reliable approach to carefully revealing real-time reaction pathways of intermediates is paramount. The graphene–molecule–graphene SMJ (GMG-SMJ) is known for its high stability, making it suitable for reaction kinetics and dynamic study.[47] For example, the Guo group's development of the GMG-SMJ opened a route towards understanding the dynamics of chemical reactions at the single-molecule level. Their recent work investigated the nucleophilic addition of NH_2OH to a carbonyl and reported strong solvent-dependent reversibility judging from the stable and sensitive real-time two steps oscillation of the current signals.[59] Additional effort has been made to elucidate the dynamics and time trajectory of unimolecular nucleophilic substitution (SN1) reaction using a 9-phenyl-9-fluorenol functional center in a GMG-SMJ.[60] The well-studied reaction involves a two-step process of heterolysis (reactant breaks to form unstable carbocation intermediate) and recombination reaction (where the carbocation intermediate reacts with a nucleophile to form a product). Due to the short lifetime of the carbocation intermediate, the dynamics of this reaction are complex and ambiguous to track. With the careful interpretation of electrical signals, they reported a reversible solvent-dependent switch in conductance corresponding to individual carbocation intermediates and reversibility of the SN1 reaction.

In another experiment, Yang *et al.* leveraged the swift temporal resolution and sensitivity of electrical current towards chemical changes to unveil the full path of the Suzuki–Miyaura cross-coupling chemical reaction.[59] The Suzuki–Miyaura reaction is a four-cascade reaction involving oxidative addition,

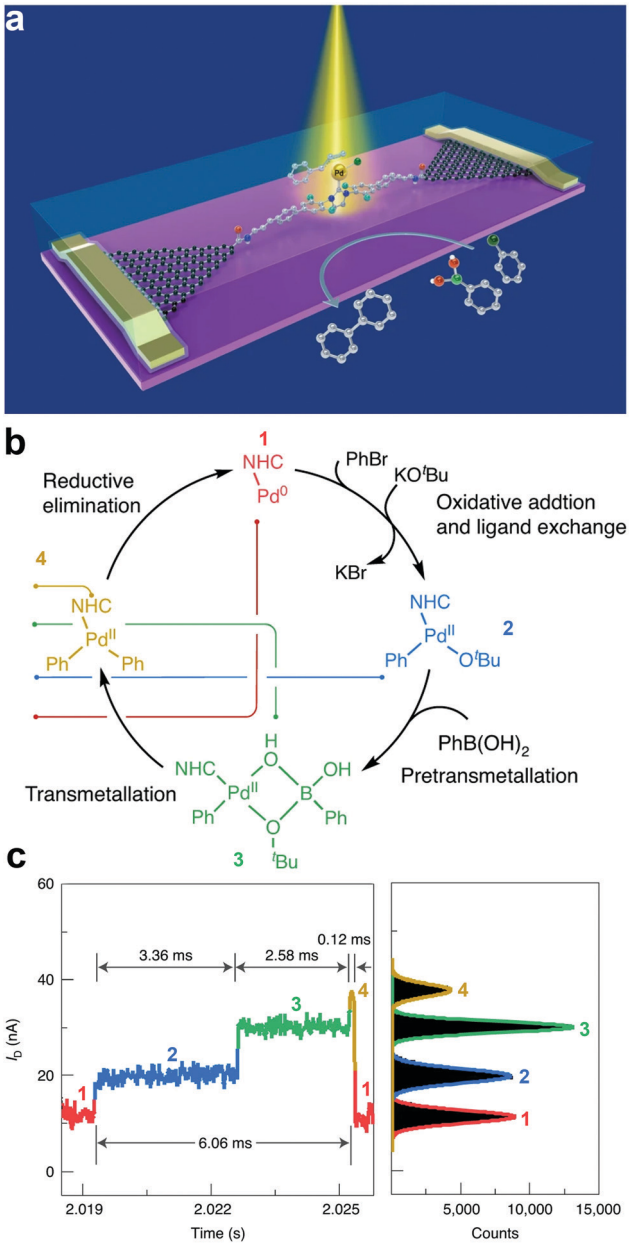

Fig. 4 (a) Schematic of a single-molecule catalytic device for the simultaneous characterization of optical, electrical characteristic, and signal attribution of the single-molecule Suzuki–Miyaura cross-coupling reaction. (b) Reaction flow attributed to the four conductance states in the current signal. From low (1) to high (4), they are 1 – Pd(0), 2 – the species after ligand exchange, the 3 – pretransmetallation species and 4 – the species before reductive elimination. (c) Current–time response of one catalytic cycle showing four conductance states and their corresponding frequency distribution (color-coded). Figures reproduced with permission from ref. 59. Copyright 2021, Springer Nature.

pretransmetallation, transmetallation, and reductive elimination reactions. However, the dynamics of the transmetalation step are unclear. In this work, a Pd-based single-molecule catalyst was trapped between two graphene electrodes to study the reaction mechanisms (Fig. 4a). Details about the reaction mechanism are presented in Fig. 4b. They reported four distinct current states corresponding to each reaction cascade. They also identified the transmetallation step as the most stable and rate-determining step (Fig. 4c). These recent efforts suggested the GMG-SMJ as a reliable platform for real-time investigation of the reaction mechanism and dynamics of organometallic catalysis.

2.4 Hosting–guest interactions

Since the introduction of the macrocycle complexes, there has been a concerted effort toward understanding the charge transport properties and mechanisms of the host–guest interactions at the SMJ interplay. The nano-diameter gap in a macrocycle complex can "host" another "guest" molecule to form a "host–guest" complex. SMJ not only helps chemists to independently separate the role of each species in electrical conductance, but it is also a formidable tool for understanding the non-covalent reaction mechanism between the host and the guest complexes.[47] The factors to consider for host–guest interactions include conductance, cavity size, linker groups, macrocycle complex/host molecule design, and affinity.[46] There are three main experimental routes to differentiating the specific role of host complexes from the guest molecules in

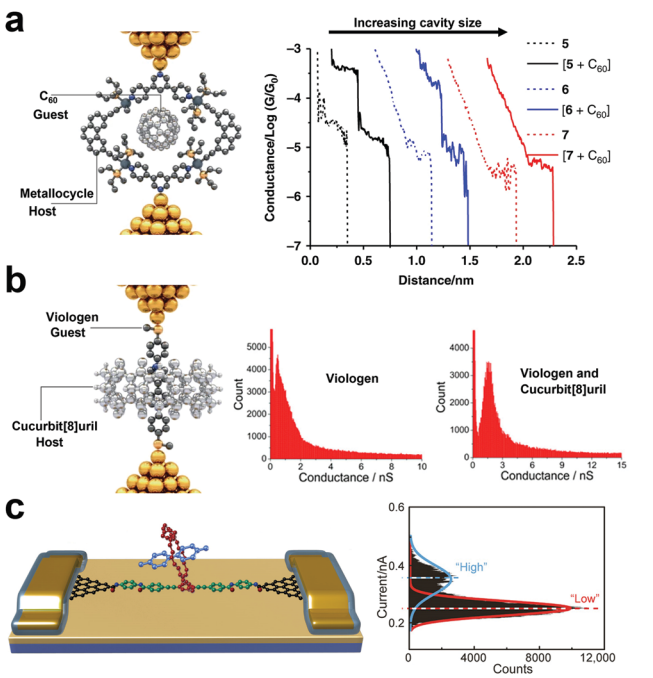

Fig. 5 (a) Schematic illustration of a C_{60}-metallocycle complex in which the macrocyclic host conducts the current (left panel). Representative conductance *vs.* distance traces of 5, 6, 7, and [5 + C_{60}], [6 + C_{60}], [7 + C_{60}] (right panel). Figures reproduced with permission from ref. 61. Copyright 2019, Springer Nature. (b) Schematic illustration of a viologen-cucurbit[8] complex in which the viologen guest conducts the current (left panel). 1D conductance histograms of viologen only and viologen-cucurbit[8] (right panel). Figures reproduced with permission from ref. 62. Copyright 2016, American Chemical Society. (c) Schematic representation of graphene point contacts. The carboxylic acid-terminated graphene point contact arrays were formed with ~2 nm gaps (left panel). Histogram of showing a bimodal current distribution (V_{bias} = 100 mV) (right panel). Figures reproduced with permission from ref. 63. Copyright 2016, American Association for the Advancement of Science.

electrical conductance. In the first route, the host macrocycle complex operates as the conducting backbone through which the conductance change is monitored when the host molecule is introduced. This configuration was exemplified by Tang *et al.*[61] They monitored the conductance of an organoplatinum(II) metallocycle host using STMBJ and studied the effect of the C_{60} guest molecule in the host cavity on the conductance change (Fig. 5a). Results showed that the conductance of the junction bearing the host–guest complex was increased by one order of magnitude relative to the guest metallocycle-only junction. They also showed strong dependence of conductance on different metallocycle cavity shapes and sizes (5, 6, and 7 corresponding to 10.87, 14.10, and 22.85 Å).

In the second route, the guest molecule bears physical contact with the top and the bottom electrode, and the introduction of the host molecules can enhance the charge carrier tunneling through space. A representative description of this route was presented by Zhang *et al*. where they measured and compared the conductance of viologen guest alone to that of cucurbit[8]uril hosting the viologen guest (Fig. 5b).[46] Relative to the viologen wire, they reported a significant rise in the viologen-cucurbit supramolecular complex induced by the change in the viologen environment.[62]

The third route is achieved by covalently attaching a macrocyclic molecule to a molecular wire to form a host complex backbone. The guest molecule is then introduced into the cavity of the host backbone. Using GMG-SMJ, Wen *et al*. investigated the thermodynamics and kinetics of conjugated molecular wire covalently bonded to a crown ether as host, with the flux of electron-deficient cation guest molecule (Fig. 5c).[63] The electron-rich crown ether in the host backbone took advantage of the electron-deficient cation guest to establish a host–guest interaction. They reported a two-step conductance profile similar to the host only and the host–guest configuration.

The same approach was adopted by Zhou *et al*. to monitor the shuttling dynamics of the pseudorotaxane supramolecular complex through temporal current responses. They covalently connected a highly conjugated molecular wire to a permethylated α-cyclodextrin macrocycle. They then shuttled the complex with dodecamethylene of different charges (positive, negative, and neutral).[64] At 300 mV source–drain bias, they reported multiple level fluctuations in conductance that is temperature and charge-dependent. For the positively charged dodecane–diamine, they observed a large number of narrowly distributed "low" conductance profiles, which indicate the downward drift of the current. The negatively charged dodecanoic acid produced narrowly distributed low "high" conductance profiles that show an upward drift of current. With the amphoteric shuttler, they observed a balance in the upward and downward drift of the current signals.

3. Harnessing quantum interference

In an SMJ, the QI effect is an intrinsic property of the wave function of a non-resonant propagating electron in the tunnelling regime. In this regime, an electron is described by a wavefunction with non-zero probability on both electrodes. The transmission function describes the probability amplitude of an electron wavefunction on the opposite electrode from its initial state. The electronic structure of the molecule behaves as a scattering center that dictates the probability amplitude of the electron wavefunction as a function of both energy and displacement.[65–70] A constructive QI is created when the scattering creates a positive interference in the electron wavefunction. The negative interference in the electron wavefunction gives rise to a destructive QI in the transmission function (Fig. 6a).[42] Controlling the wave nature of tunnelling electrons *via* tailoring molecular structures provides a unique opportunity to manipulate the electron transmission characteristics of single molecules.[71] Taking advantage of this QI effect, the charge and thermoelectric transport of single molecules can be drastically changed through subtle structural and environmental variations. This may lead to promising applications in electronics and energy conversions.[42,72]

QI in single molecules was first predicted by theoreticians more than two decades ago.[65,73,74] However, the experimental demonstrations of this effect in SMJs were absent until 2011.[66,75] In this section, we summarize recent experimental progress in detecting and tuning QI in SMJs.

Synthetic chemists are equipped with the flexibility of engineering the structure of molecules, substituting functional groups, gating, and inducing conformational changes in molecules. These effects could induce QI in single molecules. Through molecular design, Greenwald *et al*. successfully achieved high nonlinearity in charge transport of a series of benzothiadiazole (BT) flanked fluorene molecular wires by suppressing the constructive QI between the highest-occupied molecular orbital (HOMO) and lowest-unoccupied molecular orbital (LUMO) and enhancing destructive QI between the occupied molecular orbitals.[76] Their approach shows that chemical design can decouple the LUMO, and the conductance of the molecular wire was modulated up to four orders of magnitude.

Maria *et al*. trapped individual Fe-atom between two cyclopentadienyl and studied the effect of mechanically induced conformational tuning on the conductance profile.[77] They mechanically displaced the Fe-joint of the ferrocene molecule at an angle to change from the initial 1,1-Fe conformation to the 1,3-Fe conformation. As a result of destructive QI, a conductance drop by two orders of magnitude was observed as compared to their straight-chain analogy.

The direct experimental visualization of QI features in SMJs was also achieved very recently through electrochemical gating, which offered a vital strategy to utilize the QI effect. Bai *et al*. electrochemically gated a thiophene molecule showing destructive QI using an MCBJ setup.[78] At room temperature, they varied the potential of the electrochemical gate and observed a conductance minimum that implies clear evidence of charge transport modulation by anti-resonance (Fig. 6b and c). Similarly, using the STMBJ approach, Li *et al.* measured the charge transport of *meta*- and *para*-substituted diphenyl *via* electrochemical gating. They also observed the anti-resonance feature (Fig. 6d). Both

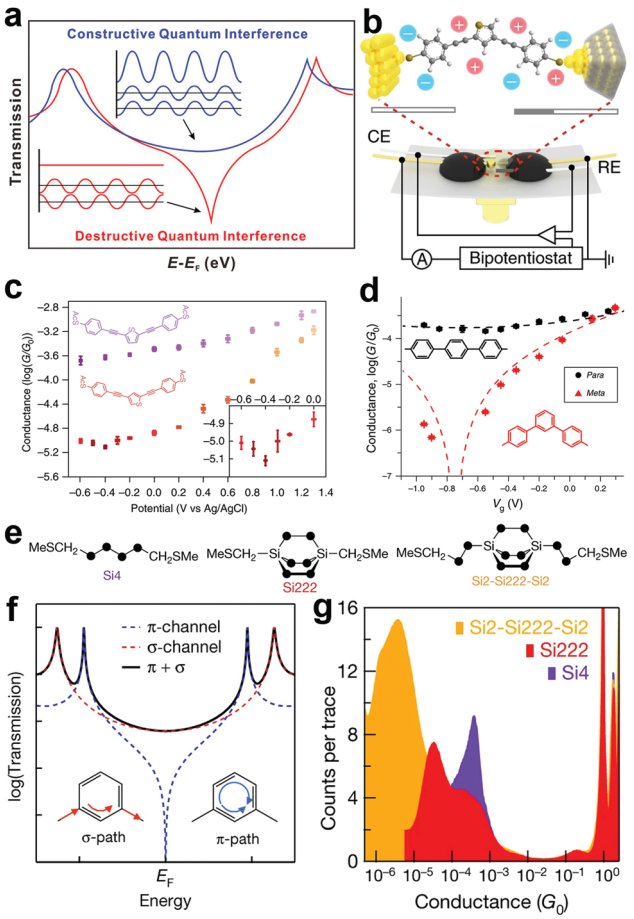

Fig. 6 (a) Schematic illustration of constructive and destructive QI. Figures reproduced with permission from ref. 42. Copyright 2019, American Chemical Society. (b) Schematics of the electrochemically gated MCBJ technique. (c) Tendency of the molecular conductance of thiothene derivative (purple) and thiophene derivative (orange) *versus* electrode potentials from −0.6 V to 1.3 V. Inset, magnification from −0.6 V to 0 V. Figures reproduced with permission from ref. 78. Copyright 2019, Springer Nature. (d) Conductance of *para* (black circles) and *meta* (red triangles). The *y* axis error bars represent standard deviations of three independent measurements; *x* axis error bars represent the potential shift of a quasi-reference electrode. Black/red dashed lines are fits of the data by simple constructive and destructive interference transmission functions. Figures reproduced with permission from ref. 79. Copyright 2019, Springer Nature. (e) DFT structures of Si222 and Si2–Si222–Si2. (f) Schematic of coherent transmission across a molecule for which there is destructive QI between contributions from different π-orbitals. (g) Logarithmically binned 1D conductance histograms for Si222, Si4 and Si2–Si222–Si2. Figures reproduced with permission from ref. 86. Copyright 2018, Springer Nature.

studies showed that conductance modulation up to two orders of magnitude could be achieved through gating the QI.[79]

To experimentally showcase the QI effect due to molecular functionalization, Wang *et al.* studied the QI effect through chemical group functionalization of 1,3,5-tris(4-aminopheynl)-benzene and its derivatives using the STMBJ.[80] They reported that molecules containing nitrogen and carbonyl showed higher conductance to about one order of magnitude compared with the alkyl substituted methyl molecule. Their observation was associated with the enhancement of the anti-resonance (shifting away from the Fermi energy) feature of the molecular orbitals due to the destructive QI effect.

The dominance of QI features on charge transport close to the Fermi energy was also demonstrated experimentally by Wang *et al.*[81] Through charge complex formation, they introduced additional constructive QI in the transmission function of thiophene-base molecules. The QI effect in their work leads to a sharp transmission peak close to the Fermi level of the electrode. As a result, a conductance that is nearly independent of molecular length, molecular backbone, and nature of electrode contact to the complexes, was observed. Their results imply that pining a constructive QI transmission feature near the electrode Fermi energy can facilitate efficient long-range charge transport through molecules.

Despite the challenges of atomic level gating in SMJ, Hong's group used STMBJ to meticulously achieve reversible switching between destructive QI and constructive QI by precise atomic gating in a series of pyridine derivatives.[82] *meta*-Connected pyridinium was reversibly protonated with CF_3COOH and deprotonated with Na_2CO_3. They also achieved irreversible methylation of the *meta*-connected pyridinium (M3-Me) and studied the conductance responses. Their report suggested that precise location protonation and methylation can interchange the frontier molecular orbitals and by extension switch interference patterns.

Another interesting approach to modulating the QI effect that has received considerable attention is varying the coupling sites of the electrode on a single molecule. Relative to the previously discussed methods, this approach is more experimentally feasible and yields more QI switching effects. Previous theoretical and experimental reports have shown that coupling electrodes to different terminals of a molecule largely influence the electronic propagation of molecules in an SMBJ setup.[37,42,83] The conventional configurations are the *-ortho*, *-para*, and the *-meta* sites.

Sriharsha *et al.* used an atomic force microscopy break junction (AFMBJ) to couple Au-electrodes to the *-para* and *-meta* sites of stilbene derivatives to study the effect of the coupling site on QI and mechanical stability of the junctions.[84] They reported wide variation in the conductance profile of both configurations. However, both *-meta* and *-para* possess similar mechanical stability.

Towards the search for an ideal single molecular insulator, the previous report has explored a decrease in transmission channel through π-orbital to showcase destructive QI. For example, in carbon-based molecular wires, destructive QI cancels transmission only in the π-route, leaving the σ-route with some lower limit conductance (Fig. 6f).[85,86] This phenomenon implies that for total insulation in a single molecule, the suppression of the σ-transmission is the key. For the first time, Garner *et al.* showed destructive QI through a σ-orbital system of saturated silicon-based molecules (Fig. 6e) using the STMBJ.[86] They showed that the conductance of Si4 is an order of magnitude higher than Si222, and that of Si222 is an order of magnitude higher than Si2-Si222-Si2 (Fig. 6g). Their work opened a new path to complete suppression of single-molecule conductance.

4. Quantifying thermal and thermoelectric transport

Beyond charge transport, thermal transport and thermoelectric energy conversion in an SMJ are receiving an increasing amount of attention as understanding them is essential for the design of thermally robust molecular circuits and high-efficiency energy conversion devices.[87–90] Theoretical studies have predicted that it is possible to achieve highly efficient thermoelectric energy conversion (*i.e.*, high thermopower and figure of merit *ZT*) in single molecules devices.[90–95] This makes SMJ an ideal testbed to examine the validity of these theoretical proposals and explore related applications. A thorough understanding of how heat is carried, dissipated, and converted in the SMJ system requires (1) experimental characterization of the thermoelectric effects (including the Seebeck and Peltier effects) and (2) direct quantification of thermal conductance of the SMJ. Thanks to the experimental advances in integrating the SMJ method with state-of-the-art thermal sensing technologies, it is now possible to directly measure thermal transport and thermoelectric energy conversion in different SMJs. In this section, we highlight recent progress in these directions.

The first experimental characterization of the Seebeck coefficient (S) of SMJs was reported by Reddy *et al*. in 2007 using an STM-based technique.[96] In their study, a temperature difference was created between a gold STM tip and the gold substrate. The open-circuit voltage of the junction containing molecules of 1,4-benzenedithiol, 4,4′-dibenzenedithiol, and 4,4″-tribenzenedithiol were measured under a series of temperature differences to derive the Seebeck coefficient of these molecules. To further enable simultaneous characterization of electrical conductance and Seebeck coefficient in an SMJ, Widawsky *et al.* later incorporated the temperature gradient setup into a conventional STMBJ measurement scheme where the thermoelectric current and electrical conductance of a single molecule can be quantified together to extract the thermovoltage produced across the SMJ.[97] Using similar techniques, the Seebeck coefficient of a wide range of molecules have been reported.[98–100]

It is expected that electrostatic gating could shift the position of frontier molecular orbitals relative to the electrode Fermi level, therefore optimizing the thermoelectric performance of SMJs. This idea was experimentally demonstrated by Kim *et al.* in 2013.[43] In their study, a microheater was embedded into one of the junction electrodes to facilitate temperature control. A back gate was introduced underneath the molecular channel in their three-terminal EBJ setup (Fig. 7a). As shown in Fig. 7b and c, the Seebeck coefficient of both the Au-biphenyldithol (BPDT)–Au junction and Au–C_{60}–Au junctions display a strong gate voltage dependence. More than a four-fold enhancement of the Seebeck coefficient was observed for the C_{60} junction. This suggests electrostatic gating as a suitable approach for improving the thermoelectric properties of SMJs. To further understand the gating effect, Gehring *et al*. simultaneously probed the conductance and thermoelectric current as a function of bias voltage and gate voltage.[101] The molecular excited states in the thermoelectric current Coulomb diamond maps indicated that the thermoelectric current was strongly asymmetric with respect to the gate voltage. Their work implies that complete thermoelectric current spectroscopy is a powerful tool for probing the ground and excited states in molecule-specific quantum transport phenomena.

In contrast to electrostatic gating, QI is considered another important avenue to enhance the thermoelectric properties as it can significantly alter the shape of the transmission characteristics near the electrode Fermi level. In a recent study, Miao *et al*. experimentally explored the influence of QI on the Seebeck coefficient of SMJs.[102] They showed that *meta*-connected oligo(phenylene ethynylene) with expected destructive interference yields a much higher S ($\sim$20 μV K^{-1}) compared to that of the *para*-connected oligo(phenylene ethynylene)3 ($\sim$10 μV K^{-1}).

The Peltier effect, the reverse of the Seebeck effect, holds promise for developing efficient thermoelectric cooling technologies. Despite the rapid progress in studying the single-molecule Seebeck effect, the characterization of the Peltier effect at the molecular scale was previously hindered by the technical challenges in detecting picowatt-level cooling. To overcome this challenge, Cui *et al*. experimentally integrated the CAFM method with custom-fabricated picowatt resolution calorimetric microdevices (Fig. 7d). Using this new approach, they achieved the unified characterization of electrical, thermoelectric, and energy dissipation characteristics of Au–biphenyl-4,4′-dithiol–Au, Au–terphenyl-4,4″-dithiol–Au, and Au–4,4′-bipyridine–Au monolayer junctions.[103] This method successfully enabled the first observation of Peltier cooling and revealed the relationship between heat dissipation and charge transmission characteristics of the SMJs (Fig. 7e and f). Although the experiments were performed on molecular monolayers, the observed cooling and heating effects are determined by the intrinsic properties of individual molecules.

The capability to quantify the thermal conductance of a molecule is of fundamental importance as it is crucial for realizing thermal management and thermoelectric energy conversion at the molecular scale. Although the thermal conductance measurement of an SMJ is conceptually straightforward, it has not been possible due to the ultra-small heat flux that can be easily concealed in the thermal noise from the measurement background. For example, the calculated thermal conductance of an SMJ is only 10–100 pW K^{-1}.[104] The technical limitation in quantifying a small heat current significantly hindered the study of single-molecule thermal transport until an important experimental breakthrough by Cui *et al*.[104–107] In their work, they integrated a high-resolution microcalorimetry into the tip of the STMBJ platform. This functionalized tip acts as both a heating and thermal sensing unit. Using this special setup, they carried out the thermal conductance measurements of Au–alkanedithiol–Au junctions.[108] The advantages of performing time-averaging measurements to increase the signal-to-noise ratio and adopting the custom-developed scanning probes with excellent mechanical stability and thermal sensitivity made it possible to quantify very small thermal current through single

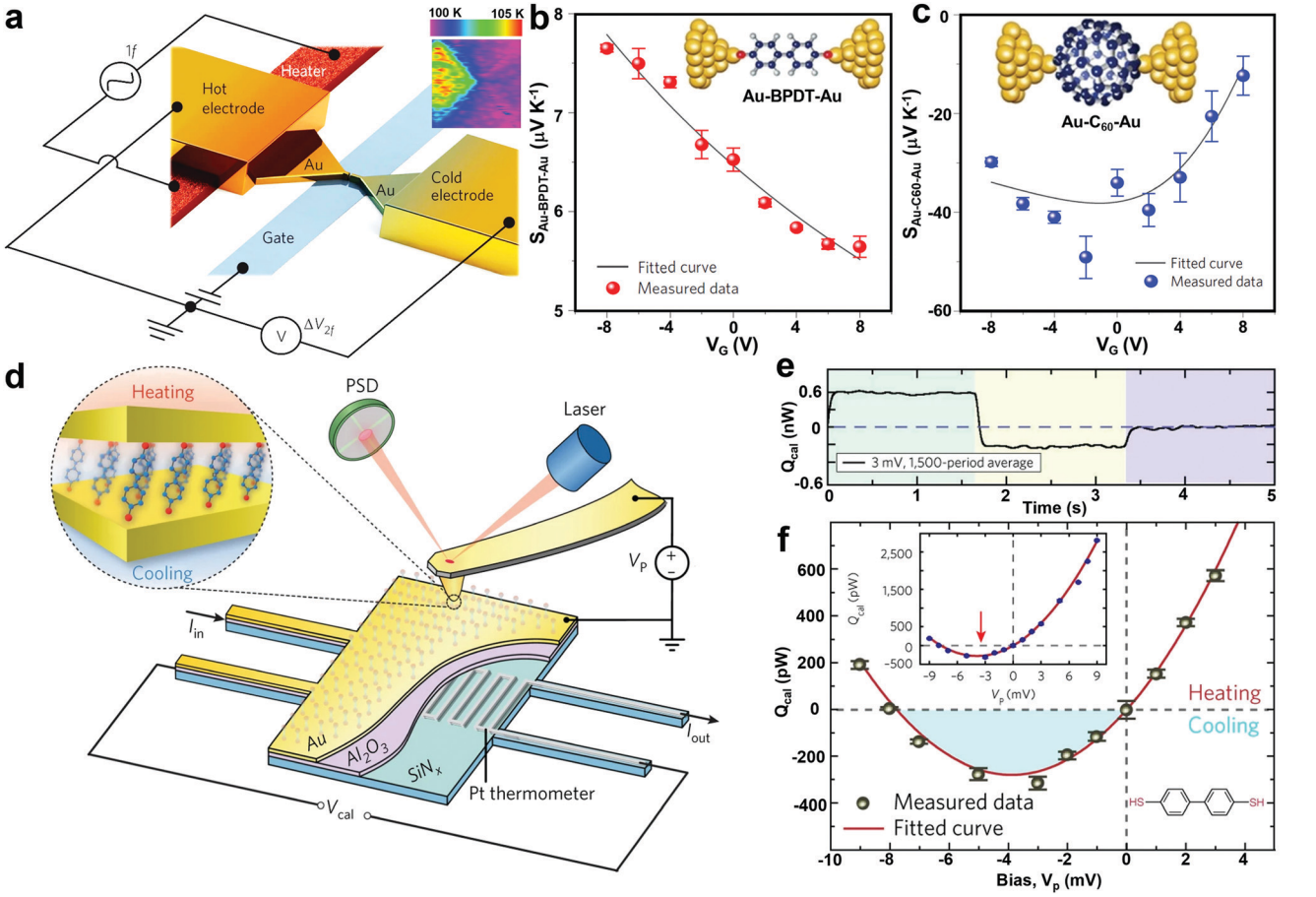

Fig. 7 (a) Schematic of the EBJs with an integrated heater (red) and a gate electrode (blue) for modulating thermoelectricity in molecular junctions *via* electrostatic gating. Insert: thermal map of a nanogap junction obtained using scanning thermal microscopy. (b and c) Measured Seebeck coefficient as a function of gate voltage V_G for Au–BPDT–Au (upper) and Au–C_{60}–Au (lower) junctions. Figures reproduced with permission from ref. 43. Copyright 2014, Springer Nature. (d) Schematic of the platform that molecular junctions are formed by placing an Au-coated AFM probe in gentle contact with a self-assembled monolayer created on an Au-coated calorimetric microdevice. (e) A representative example of quantifying the heating and cooling power in molecular junctions by averaging the thermal signal over a large number of periods to reduce the noise level. (f) Measured voltage-dependent thermal power for biphenyl-4,4′-dithiol junctions. The shaded blue region indicates the net cooling (refrigeration) observed. Inset shows full range data from −9 to 9 mV. Figures reproduced with permission from ref. 103. Copyright 2018, Springer Nature.

molecules (Fig. 8a). The temperature resolution of their measurement platform reached around 0.1 mK, which enabled the detection of thermal conductance with a resolution of ≈ 2 pW K^{-1} root mean square (Fig. 8b). Interestingly, the thermal conductance of Au–alkanedithiol–Au junctions with the number of carbon atoms varying from two to ten is nearly independent of molecular length, although their electrical conductance decreases exponentially (Fig. 8c).

In 2019, another group combined the BJ technique with suspended heat-flux sensors with picowatt per Kelvin sensitivity, to measure the thermal and electrical conductance of single dithiol-oligo(phenylene ethynylene) and octane dithiol MJs at room temperature simultaneously.[109] Heat transport through these junctions was governed by the phonon mismatch between the molecules and the metallic electrodes. It is promising to extend these techniques to other short molecules, polymer chains, and low-dimensional nanostructures for accurate thermal conductance characterization.

Currently, the major challenge in broad thermoelectric applications of MJs lies in low efficiency (*i.e.*, high power factor G_eS^2 and figure of merit ZT). Improving ZT requires an appropriate design to enhance the electrical conductance and Seebeck coefficient of an SMJ while significantly suppressing its thermal conductance. Knowledge gained from recent studies implies that proper use of external gating and/or the QI effect can be a promising strategy to achieve these requirements in future investigations.

5. Controlling electron spins

In contrast to the electron's charge, the electron's spin carries information encoded in its spin state. Compared to conventional inorganic spintronic materials, such as semiconductors or metals, molecules offer more fabulous room for spin manipulation due to their structural flexibility and diversity. Equally

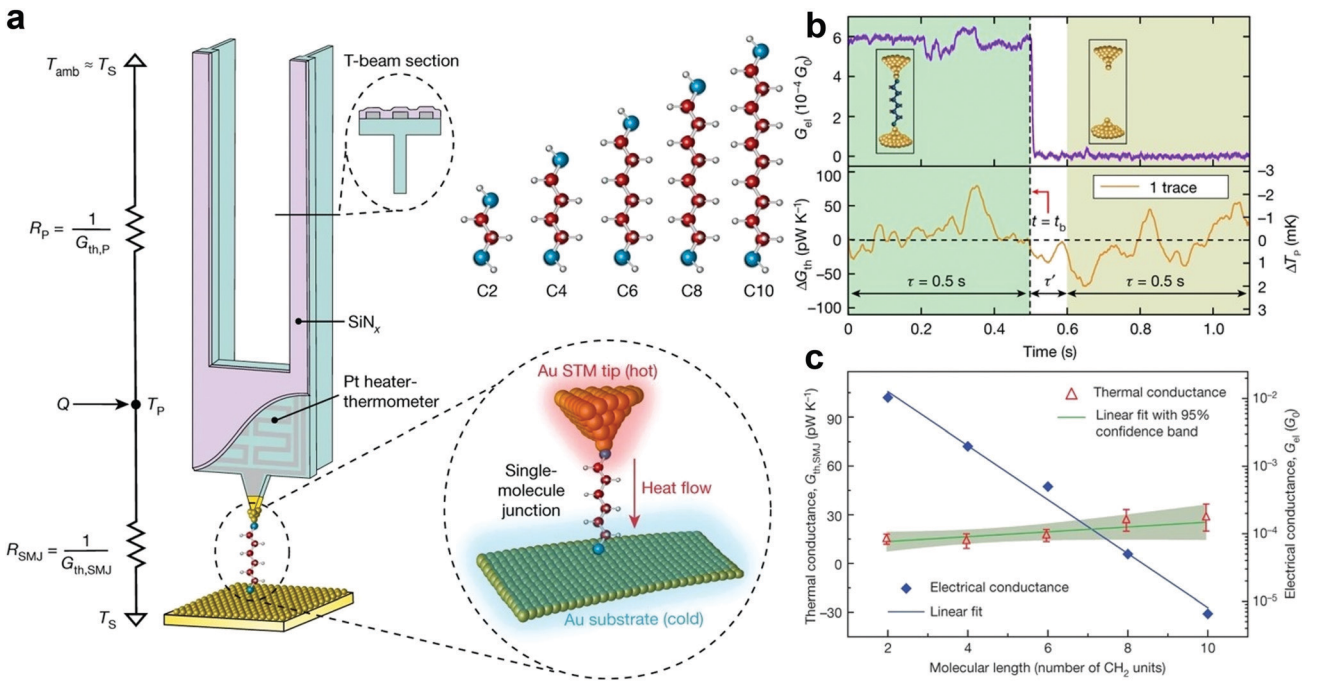

Fig. 8 (a) Schematic of the calorimetric scanning thermal microscopy setup for thermal conductance measurements of single Au–alkanedithiol–Au molecular junctions. The Au-coated tip is heated by an embedded Pt heater-thermometer. C2, C4, C6, C8, and C10 alkanedithiol molecules are studied in this work. (b) Experimental strategy for measuring the thermal conductance of a single-C6 junction by recording the electrical conductance trace (upper panel) and the thermal conductance change (ΔG_{th}) simultaneously. (c) Measured electrical and thermal conductance as a function of the molecular length, as given by the number of CH_2 units in the alkanedithiol junctions. Figures reproduced with permission from ref. 108. Copyright 2019, Springer Nature.

importantly, molecular-scale spintronics represents the ultimate miniaturization of spin-based devices and holds promise for future quantum information technologies. In addition, spin properties that have no analogy in conventional materials, such as the spin selectivity induced by molecular chirality, have been discovered in various molecular-scale systems. This section concentrates on recent progress investigating the CISS effect and spin-dependent transport in SMJs.

5.1 Chiral induced spin selectivity in chiral molecules

The CISS effect refers to the preferential transfer of electrons with one spin orientation over the other across chiral molecules and materials (Fig. 9a).[110–112] Chiral molecules are the focus of intensive research in chemistry, driven primarily by pharmaceutical applications. For chiral molecules, CISS results in preferential electron spin orientation in the molecular frame. Thus, spin selection rules are an important consideration for chemical transformations involving chiral species.[112]

As one of the early efforts in probing the CISS effect, Xie *et al.* measured spin specific electron conduction through double-stranded DNA molecules for spin-polarized electrons injected either parallel or antiparallel to the helical axis using a CAFM technique.[44] The experimental setup is shown in Fig. 9b. The CAFM tip was used to measure the current–voltage (I–V) curves of an Au nanoparticle–dsDNA–nickel junction under different magnetization polarities of the Ni substrate. Average I–V curves (Fig. 9c) clearly show that the molecular conductance strongly depends on the direction of the external magnetic field, suggesting spin selective electron transport.

Although the CISS effect is often attributed to the interplay between spin–orbit interactions and the chirality within the molecule, such an explanation requires unrealistically large molecular spin–orbit interaction. Therefore, the appropriate interpretation of the observed CISS effect was given by Seif Alwan *et al.*[113] They suggested that the origin of the CISS effect was the interplay between the chirality-induced solenoid field in the molecule, the presence of large spin–orbit coupling in the electrode, and a spin-transfer torque effect between the chiral molecule and the electrode. Their phenomenological theory can qualitatively account for all critical experimental observations for the molecular junctions, most notably the magnitude of the CISS with realistic parameters.

In general, the CISS effect offers a way to harness spin-polarized electrons. It opens new possibilities for different spintronic applications, in which most devices are currently built with inorganic magnetic materials. Using a single molecular layer as the spin filter promises more remarkable energy efficiency and miniaturization in device size. Another significant direction is the investigation of the CISS effect in biology. Although numerous biological electron transfer processes take place through chiral systems, the role of the CISS effect has not yet been fully concerned.

5.2 Spin transport in SMJs

Besides the CISS effect, the single molecular magnets in contact with metal electrodes provide another exciting playground and

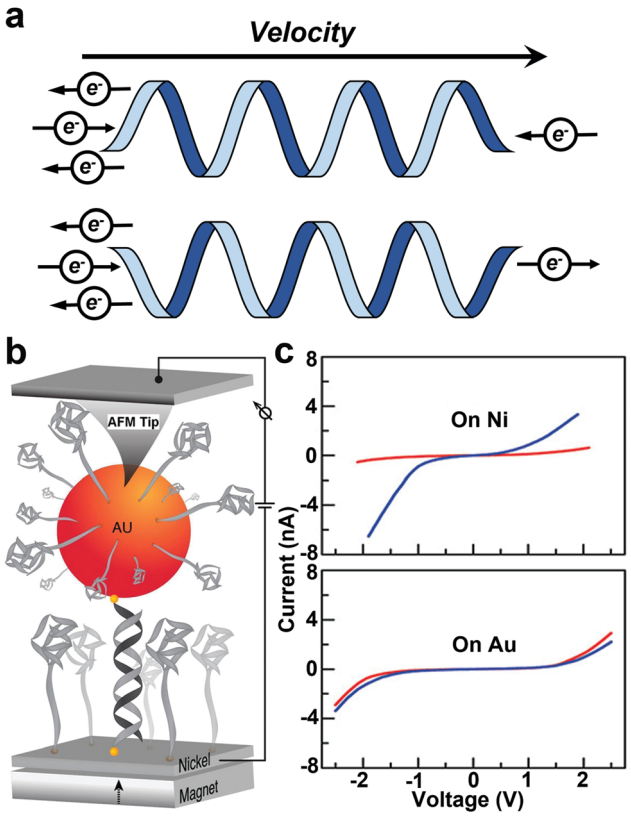

Fig. 9 (a) Schematic diagram of the CISS effect. (b) A schematic of the experimental setup to measure the conductance of an Au nanoparticle–dsDNA–nickel molecular junction. Current is measured between the nickel substrate and the tip of the AFM. (c) The average current obtained for the three oligomers studied when the magnetic field points up (red) or down (blue). The bottom panel is the control experiment with a gold substrate instead of nickel. Figures reproduced with permission from ref. 44. Copyright 2011, American Chemical Society.

abundant physics to study spin-dependent transport properties through a single molecule. We here focus on the recent experiments attempting to detect and control the spin state of a molecule and the spin electrons flowing through SMJs.

Introducing spin sensitivity through functionalization by a magnetic molecule offered the possibility of producing spin excitations on the tip apex of an STM. Verlhac *et al.* fabricated a nickelocene-terminated tip (Nc-tip).[114] When it was 100 picometers away from point contact with a surface-supported object, magnetic effects could be probed through changes in the spin excitation spectrum of nickelocene. This detection scheme can simultaneously determine the exchange field, and the spin polarization of iron atoms and cobalt films on a copper surface with atomic-scale resolution.

Interestingly, Atindra *et al.* recently showed that spin-polarized currents were generated in single silver–vanadocene–silver junctions without magnetic components or magnetic fields.[115] The conductance approached the ideal ballistic spin transport limit in some cases, where it was primarily dominated by an almost fully open spin-polarized transmission channel. Such efficient spin filtering in a non-magnetic nanoscale system leads to fast and power-saving spin-current manipulations.

The quantum mechanical ground state becomes particularly important in a nanoscale junction device as various new physical phenomena could emerge. An exceptional current-blockade phenomenon called ground-state spin blockade occurs when the ground state spin of subsequent charge states differs by more than 1/2. Sequential electron tunneling transitions between these ground states are forbidden by the spin selection rules, and Coulomb blockade peaks are suppressed. Bruijckere *et al.* presented a direct experimental demonstration of a ground-state spin blockade in a high spin single pyridine functionalized Mn(iii) Anderson polyoxometalate molecule transistor at zero external magnetic field (Fig. 10a), as the measured transport characteristics exhibited a complete suppression of resonant transport due to a ground-state spin difference of 3/2 between subsequent charge states.[116] Remarkably, the blockade can be reversibly lifted by applying with an external magnetic field. Furthermore, Mitchell *et al.* unified QI and Kondo effect phenomena in SMJs and showed that transport through a spin-degenerate molecule can be either enhanced or blocked by Kondo correlations, depending on the molecular structure, contacting geometry, and applied gate voltages.[117] This research illustrates the intricate interplay of quantum effects beyond the single-orbital paradigm.

Molecular magnetic switches (or spin switches) are one of the most crucial components in molecule-based spintronics for future quantum information processing and storage. Recent progress demonstrated reversible switching in molecular junctions *via* various external stimuli such as force field, bias voltage, and magnetic field.[118] Aragonès *et al.* presented a single molecule Fe^{II} complexes wire that displayed significant conductance switching (>2 orders of magnitude) by controlling the spin-dependent transport under ambient conditions (room temperature in a liquid cell) when the electrons flow from the Au electrode to either an α-up or a β-down spin-polarized Ni electrode.[119] Another example is the reversible control of the oxidation and spin state in a single iron(iii) octaethylporphyrin chloride (Fe-OEP-Cl) molecule in the force field induced by an STM tip, which can determine its chemical reactivity and magnetic properties.[120] Not only do the external forces open pathways for controlling magnetic properties of molecular junctions, but a bias voltage could be used to switch two states in a single magnetic molecule with a coupled spin pair (Fig. 10b).[121] In particular, they used the MCBJ technique to measure electronic transport through an SMJ containing two coupled spin centers confined to two Co ions. A finite bias can drive switching of the transition from the pseudo-singlet ground state of a coupled spin system to a pseudo-triplet state at higher bias voltage, while these states are assigned to the absence and occurrence of a Kondo-like zero-bias anomaly. In addition, Kai *et al.* exhibited that the electron pathway in a single iron phthalocyanine (FePc) molecule device can be tuned at very low energy between two molecular orbitals by varying the external magnetic field, giving rise to a tunable anisotropic magnetoresistance up to 93% (Fig. 10c).[122] This unique tunability of the electron pathways originates from the reorientation of the magnetic moment on the metal center, resulting in a

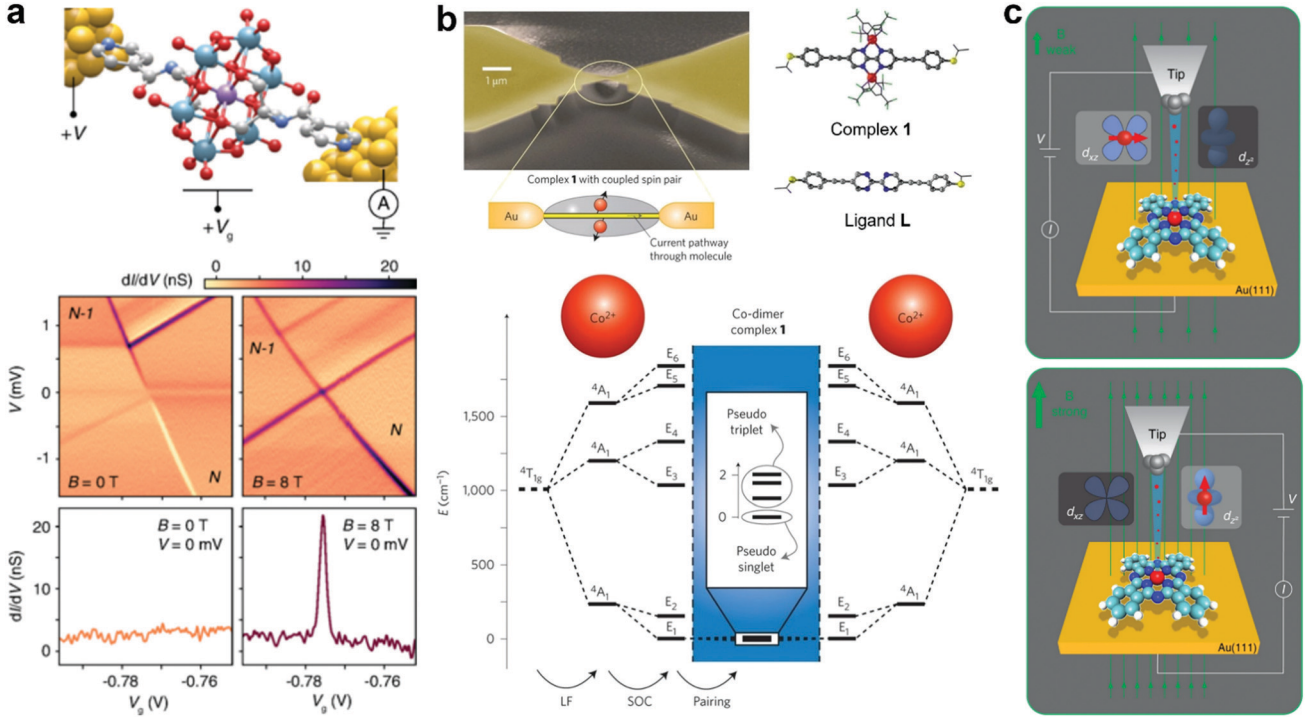

Fig. 10 (a) Top: a sketch of the pyridine functionalized Mn(III) Anderson polyoxometalate MJ. Bottom: d*I*/d*V* maps at zero magnetic field and 8 T as a function of bias voltage (*V*) and gate voltage (V_g), no sequential electron tunnelling lines at 0 T due to the ground-state spin blockade. Figures reproduced with permission from ref. 116. Copyright 2019, American Physical Society. (b) Top: scheme and SEM micrograph of the SMJ with a pair of spin centers (Co^{2+} ions). Molecular structure of complex **1** and bare bipyrimidine-wire **L** (for control experiments). Bottom: Electronic states of the coupled spin system from quantum chemical calculations. Figures reproduced with permission from ref. 121. Copyright 2013, Springer Nature. (c) Schematics of the electron transport through a FePc molecule adsorbed on the Au(111) surface at different magnetic fields. The spin direction of Fe is in-plane, and currents flow by the d_{xz}/d_{yz} orbital at a weak magnetic field. In contrast, Fe spin is aligned to the magnetic field, and electrons tunnel preferentially through the d_{z^2} orbital at a strong magnetic field. Figures reproduced with permission from ref. 122. Copyright 2019, Springer Nature.

re-hybridization of molecular orbitals. Therefore, these external stimuli can be employed to control the single-electron process in a single-molecule device or molecular spintronics.

6. Revealing structural fingerprint using Raman spectroscopy

The geometrical structure of the molecule in the nanogap and the way it binds with the electrodes have a critical impact on the transport properties of the molecule. However, this important structural information is hardly accessible from the conventional SMJ electrical measurements. To overcome this challenge, recent experimental efforts have attempted to develop approaches that combine Raman spectroscopy with the SMJ method. This is primarily because Raman spectroscopy enables the detection of detailed bond vibrational modes within a molecule and therefore provides a structural fingerprint of the junction. Using this new approach, it is feasible to carry out *in situ* observation of structure–property relations and dynamics of a single molecule by recording the electrical and spectroscopic signals simultaneously. This section presents experimental progress in using different SMJ-Raman spectroscopy-based techniques.

Liu *et al.* first introduced a technique named "fishing-mode" tip-enhanced Raman spectroscopy (FM-TERS), in which molecule-to-surface bonding can be characterized simultaneously during electron transport at room temperature (Fig. 11a).[45] The TERS spectra and the conductance dynamics of 4bipy were acquired at the same time by FM-TERS (Fig. 11b and c). The ν_{8a} Raman band of 4bipy depended on the junction bias, and the band split in the nonlinear region of the *I*–*V* curve, which was ascribed to the shortening of the Au–N bond between the drain gold electrode and its closest pyridine ring at a high bias. This approach has been demonstrated to be highly efficient and simple for investigating the relationships between structural, electrical, and optical properties of various materials. Later, another technique with dual characterization functions called MCBJ-based surface-enhanced Raman spectroscopy (MCBJ-SERS) was developed to measure single 4,4′-bipyridine SMJ in solution.[123] They observed the dynamics of a single molecule's motion between vertical and tilting junction configurations through the b1 and b2 modes switching in the collected Raman spectra. A slight increase in the tilting angle of the molecule in junctions leads to a decrease in the conductance of the SMJ. As shown in Fig. 11d, Guo *et al.* recently employed a modified MCBJ-SERS technique with a third electrode as the gate control.[124] They demonstrated that the Raman intensity of 1,4-benzenedithiol in the junction could be tuned by electromagnetic gating with a 40% Raman intensity enhancement (Fig. 11e).

Besides the FM-TERS and MCBJ-SERS measurement platforms, Jeong *et al.* fabricated a MEMS-based break junction

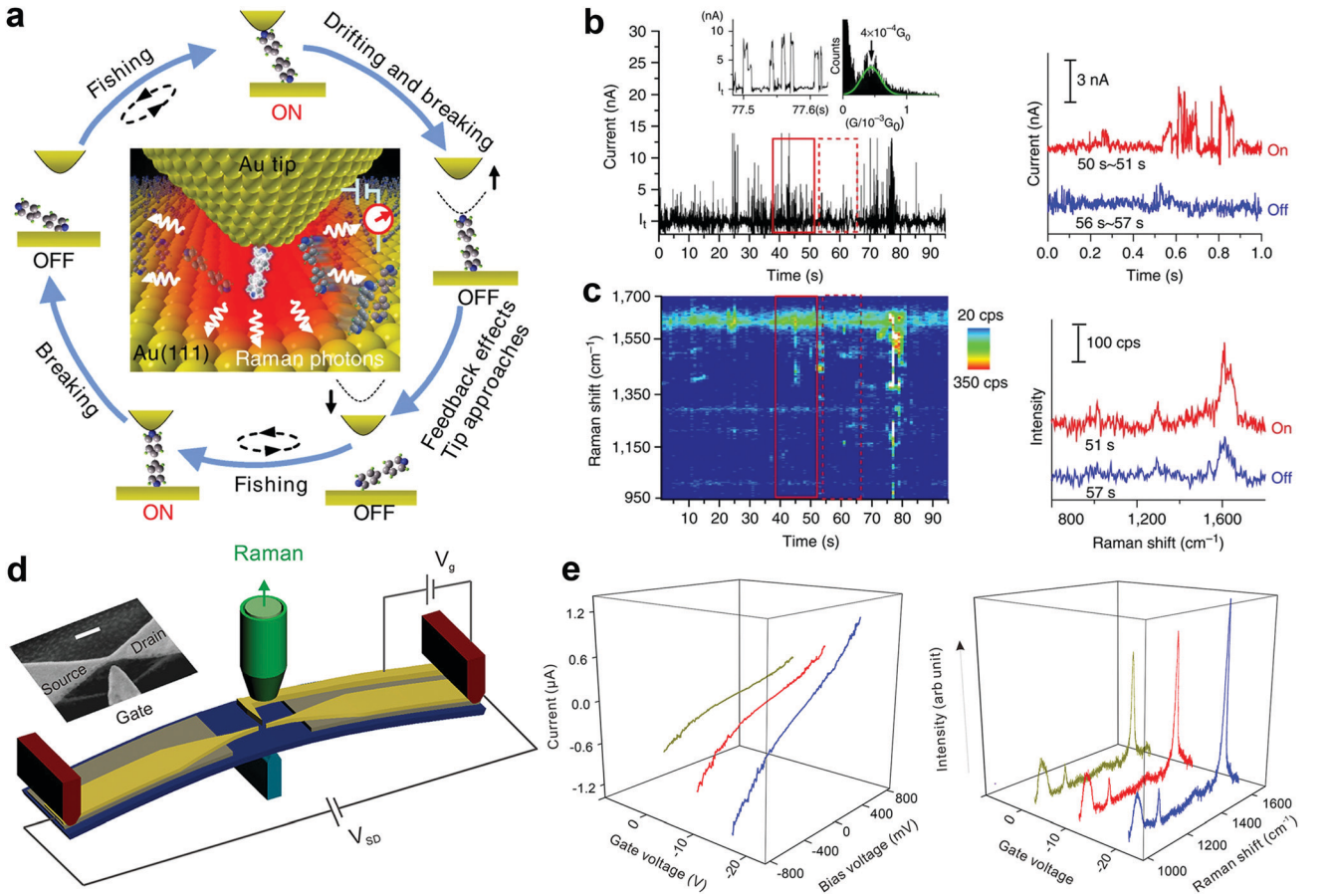

Fig. 11 (a) A schematic illustration of the 'fishing-mode' TERS. (b and c) Simultaneous conductance and TERS measurement of 4bipy by 'fishing-mode' TERS. Upper: Conductance *versus* time; Lower: TERS spectra *versus* time. Figures reproduced with permission from ref. 45. Copyright 2011, Springer Nature. (d) Experimental schematic of side-gating Raman scattering. Scale bar is 100 nm for the inset SEM image of the MCBJ chip with a side-gate electrode. (e) SERS spectra recorded at different gate voltages (left panel) and *I*–*V* curves of 1,4-benzenedithiol MJ upon different gate voltages (right panel). Figures reproduced with permission from ref. 124. Copyright 2018, American Chemical Society.

(MEMS-BJ) device coupled with Raman spectroscopy to perform real-time on-chip electrical, optical, and mechanical characterization of MJs.[125,126] This on-chip platform reached sub-nanometer mechanical resolution over a wide temperature range. This technique offers opportunities to achieve high-throughput electrical characterization of single-molecule devices.

However, a potential drawback of the techniques introduced above is that the total Raman scattering intensity from the tip area is very weak due to the substrate and morphology limitations of SERS. The shell isolated nanoparticle-enhanced Raman spectroscopy (SHINERS) technique was invented and used in MJ research to overcome this issue. Yu *et al.* recently combined the STMBJ technique and SHINERS to probe the solvent-induced interfacial effects on molecular adsorption at atomically flat surfaces.[127] SHINERS provided direct spectroscopic evidence of adsorption geometry modulation at the Au(111) surface.

To date, several approaches that combined Raman spectroscopy with SMJ techniques, including TERS, MCBJ-SERS, MEMSBJ-SERS, and SHINERS, have been proven to be capable of directly monitoring conformational change, chemical reaction, and molecule/electrode interface coupling in SMJs. We expect that future experimental efforts will be devoted to improving the spatial and temporal resolution and efficiency of these single-molecule Raman spectroscopy methods with the goal of mapping the complete physical and chemical fingerprints of the SMJ.

7. Conclusion and outlook

In the early days, the development of molecular electronics was energetically channeled to the measurement of molecular conductance. The continuous effort in improving and expanding the capabilities of SMJ techniques has now enabled the previously unachievable investigation of a variety of interesting physical and chemical properties beyond electrical conductance. These emerging techniques and methodologies have opened a new avenue for gaining molecular-level insights into fundamental questions that may have a profound impact on research areas beyond molecular electronics, including but not limited to, synthetic chemistry, materials science, energy harvesting, and computing. In this perspective, we underscore the uniqueness

and versatility of SMJ techniques for single-molecule studies and draw attention from related research communities to adopt suitable SMJ measurements in their future studies.

When SMJs are equipped with knowledge from other related disciplines, one can see their tremendous potential as a powerful tool to attain information on the fundamental mechanisms of a certain physical or chemical process with single-molecule sensitivity. By categorizing recent achievements, we have highlighted the remarkable advances in using SMJs to understand single-molecule processes associated with chemical reactions, quantum transport, energy conversion, spintronics and more. Despite this promising progress, fundamental questions remain to be answered. For example, in electric field-driven chemical reactions, a deeper understanding of the reaction selectivity and how the experimental insights can be transferred to bulk synthetic chemistry is required. Similarly, while several molecules with constructive or destructive interference properties have been reported, it is still difficult to precisely control the energy position of these QI features, which is essential for achieving highly efficient long-range transport and thermoelectric energy conversion. Furthermore, developing strategies to control molecular spin at room temperature is imperative. We note that in parallel to exploring new molecular systems and applications, it is equally important to address the fundamental questions associated with them.

In conclusion, the availability of rich functional molecules, novel SMJ experimental ideas, and ingenious implementation of these ideas have led to the rapid growth of new research directions beyond electrical conductance. There is no doubt that the intimate collaborations among synthetic chemists, experimental physicists, nanoengineers, and theorists will continue to push the frontiers of these directions and explore new applications yet to be imagined. It is expected that the SMJ, as a fertile platform bridging gaps of distinct disciplines, may offer a shortcut toward addressing crucial fundamental problems in chemistry, materials science, energy conversion, and information technologies.

Conflicts of interest

There are no conflicts to declare.

Acknowledgements

We acknowledge the financial support from the U.S. Department of Energy Basic Energy Sciences Division (DE-SC0021942) and the National Science Foundation (OIA-1757220).

References

1 A. Aviram and M. A. Ratner, *Chem. Phys. Lett.*, 1974, **29**, 277–283.
2 R. H. M. Smit, Y. Noat, C. Untiedt, N. D. Lang, M. C. van Hemert and J. M. van Ruitenbeek, *Nature*, 2002, **419**, 906–909.
3 Y. Xue, S. Datta and M. A. Ratner, *Chem. Phys.*, 2002, **281**, 151–170.
4 M. Brandbyge, J. L. Mozos, P. Ordejón, J. Taylor and K. Stokbro, *Phys. Rev. B: Condens. Matter Mater. Phys.*, 2002, **65**, 1654011–16540117.
5 L. Venkataraman, J. E. Klare, C. Nuckolls, M. S. Hybertsen and M. L. Steigerwald, *Nature*, 2006, **442**, 904–907.
6 K. Wang and B. Xu, *Top. Curr. Chem.*, 2017, **375**, 17.
7 J. O. Thomas, B. Limburg, J. K. Sowa, K. Willick, J. Baugh, G. A. D. Briggs, E. M. Gauger, H. L. Anderson and J. A. Mol, *Nat. Commun.*, 2019, **10**, 4628.
8 K. Liu, X. Wang and F. Wang, *ACS Nano*, 2008, **2**, 2315–2323.
9 G. Binnig and H. Rohrer, *IBM J. Res. Dev.*, 1986, **30**, 355–369.
10 D. Xiang, H. Jeong, T. Lee and D. Mayer, *Adv. Mater.*, 2013, **25**, 4845–4867.
11 F. J. Giessibl, *Rev. Mod. Phys.*, 2003, **75**, 949–983.
12 W. Liang, M. P. Shores, M. Bockrath, J. R. Long and H. Park, *Nature*, 2002, **417**, 725–729.
13 Y. Li, C. Yang and X. Guo, *Acc. Chem. Res.*, 2020, **53**, 159–169.
14 B. Xu and N. J. Tao, *Science*, 2003, **301**, 1221–1223.
15 X. Qiu, S. Rousseva, G. Ye, J. C. Hummelen and R. C. Chiechi, *Adv. Mater.*, 2021, **33**, 2006109.
16 M. Y. Ni, H. L. Wang, L. X. Cheng, C. Q. Sheng, X. Peng, K. Deng, C. M. Wang, R. F. Chen, Q. D. Zeng and J. H. Wan, *Appl. Surf. Sci.*, 2021, **537**, 147313.
17 G. P. Zhang, L. Y. Chen, J. M. Zhao, Y. Z. Sun, N. P. Shi, M. L. Wang, G. C. Hu and C. K. Wang, *J. Phys. Chem. C*, 2021, **125**, 20783–20790.
18 H. Nakamura, Y. Asai, J. Hihath, C. Bruot and N. Tao, *J. Phys. Chem. C*, 2011, **115**, 19931–19938.
19 S. K. Yee, J. Sun, P. Darancet, T. D. Tilley, A. Majumdar, J. B. Neaton and R. A. Segalman, *ACS Nano*, 2011, **5**, 9256–9263.
20 I. Díez-Pérez, J. Hihath, Y. Lee, L. Yu, L. Adamska, M. A. Kozhushner, I. I. Oleynik and N. Tao, *Nat. Chem.*, 2009, **1**, 635–641.
21 M. Elbing, R. Ochs, M. Koentopp, M. Fischer, C. V. Hänisch, F. Weigend, F. Evers, H. B. Weber and M. Mayor, *Proc. Natl. Acad. Sci. U. S. A.*, 2005, **102**, 8815–8820.
22 R. M. Metzger, B. Chen, D. Vuillaume, M. V. Lakshmikantham, U. Höpfner, T. Kawai, J. W. Baldwin, X. Wu, H. Tachibana, H. Sakurai and M. P. Cava, *J. Am. Chem. Soc.*, 1998, **43**, 10455–10466.
23 A. Polakovsky, J. Showman, J. Valdiviezo and J. L. Palma, *Phys. Chem. Chem. Phys.*, 2021, **23**, 1550–1557.
24 M. L. Perrin, E. Burzurí and H. S. J. Van Der Zant, *Chem. Soc. Rev.*, 2015, **44**, 902–919.
25 S. Richter, E. Mentovich and R. Elnathan, *Adv. Mater.*, 2018, **30**, 1706941.
26 M. Kalla, N. R. Chebrolu and A. Chatterjee, *Sci. Rep.*, 2021, **11**, 10458.
27 P. Gehring, J. K. Sowa, J. Cremers, Q. Wu, H. Sadeghi, Y. Sheng, J. H. Warner, C. J. Lambert, G. A. D. Briggs and J. A. Mol, *ACS Nano*, 2017, **11**, 5325–5331.
28 J. Kushmerick, *Nature*, 2009, **462**, 994–995.

29 Y. H. Wang, F. Yan, D. F. Li, Y. F. Xi, R. Cao, J. F. Zheng, Y. Shao, S. Jin, J. Z. Chen and X. S. Zhou, *J. Phys. Chem. Lett.*, 2021, **12**, 758–763.
30 J. Li, Q. Wu, W. Xu, H.-C. Wang, H. Zhang, Y. Chen, Y. Tang, S. Hou, C. J. Lambert and W. Hong, *CCS Chem.*, 2021, **3**, 1744–1752.
31 S. Y. Quek, M. Kamenetska, M. L. Steigerwald, H. J. Choi, S. G. Louie, M. S. Hybertsen, J. B. Neaton and L. Venkataraman, *Nat. Nanotechnol.*, 2009, **4**, 230–234.
32 P. Liljeroth, J. Repp and G. Meyer, *Science*, 2007, **317**, 1203–1206.
33 E. Lörtscher, J. W. Ciszek, J. Tour and H. Riel, *Small*, 2006, **2**, 973–977.
34 F. Chen, J. He, C. Nuckolls, T. Roberts, J. E. Klare and S. Lindsay, *Nano Lett.*, 2005, **5**, 503–506.
35 T. Gao, Z. Pan, Z. Cai, J. Zheng, C. Tang, S. Yuan, S. Qiang Zhao, H. Bai, Y. Yang, J. Shi, Z. Xiao, J. Liu and W. Hong, *Chem. Commun.*, 2021, **57**, 7160–7163.
36 M. Ratner, *Nat. Nanotechnol.*, 2013, **8**, 378–381.
37 S. V. Aradhya and L. Venkataraman, *Nat. Nanotechnol.*, 2013, **8**, 399–410.
38 J. Zhang, P. Chen, B. Yuan, W. Ji, Z. Cheng and X. Qiu, *Science*, 2013, **342**, 611–614.
39 Y. Chen, L. Huang, H. Chen, Z. Chen, H. Zhang, Z. Xiao and W. Hong, *Chinese J. Chem.*, 2021, **39**, 421–439.
40 I. Stone, R. L. Starr, Y. Zang, C. Nuckolls, M. L. Steigerwald, T. H. Lambert, X. Roy and L. Venkataraman, *Nat. Rev. Chem.*, 2021, **5**, 695–710.
41 C. Jia, B. Ma, N. Xin and X. Guo, *Acc. Chem. Res.*, 2015, **48**, 2565–2575.
42 J. Liu, X. Huang, F. Wang and W. Hong, *Acc. Chem. Res.*, 2019, **52**, 151–160.
43 Y. Kim, W. Jeong, K. Kim, W. Lee and P. Reddy, *Nat. Nanotechnol.*, 2014, **9**, 881–885.
44 Z. Xie, T. Z. Markus, S. R. Cohen, Z. Vager, R. Gutierrez and R. Naaman, *Nano Lett.*, 2011, **11**, 4652–4655.
45 Z. Liu, S.-Y. Ding, Z.-B. Chen, X. Wang, J.-H. Tian, J. R. Anema, X.-S. Zhou, D.-Y. Wu, B.-W. Mao, X. Xu, B. Ren and Z.-Q. Tian, *Nat. Commun.*, 2011, **2**, 305.
46 H. Chen and J. Fraser Stoddart, *Nat. Rev. Mater.*, 2021, **6**, 804–828.
47 X. Xie, P. Li, Y. Xu, L. Zhou, Y. Yan, L. Xie, C. Jia and X. Guo, *ACS Nano*, 2022, **16**, 3476–3505.
48 R. Meir, H. Chen, W. Lai and S. Shaik, *ChemPhysChem*, 2010, **11**, 301–310.
49 S. Shaik, S. P. De Visser and D. Kumar, *J. Am. Chem. Soc.*, 2004, **126**, 11746–11749.
50 S. Ciampi, N. Darwish, H. M. Aitken, I. Díez-Pérez and M. L. Coote, *Chem. Soc. Rev.*, 2018, **47**, 5146–5164.
51 S. Shaik, D. Mandal and R. Ramanan, *Nat. Chem.*, 2016, **8**, 1091–1098.
52 A. C. Aragonès, N. L. Haworth, N. Darwish, S. Ciampi, N. J. Bloomfield, G. G. Wallace, I. Diez-Perez and M. L. Coote, *Nature*, 2016, **531**, 88–91.
53 C. Yang, Z. Liu, Y. Li, S. Zhou, C. Lu, Y. Guo, M. Ramirez, Q. Zhang, Y. Li, Z. Liu, K. N. Houk, D. Zhang and X. Guo, *Sci. Adv.*, 2021, **7**, eabf0689.
54 X. Huang, C. Tang, J. Li, L. C. Chen, J. Zheng, P. Zhang, J. Le, R. Li, X. Li, J. Liu, Y. Yang, J. Shi, Z. Chen, M. Bai, H. L. Zhang, H. Xia, J. Cheng, Z. Q. Tian and W. Hong, *Sci. Adv.*, 2019, **5**, eaaw3072.
55 Y. Zang, Q. Zou, T. Fu, F. Ng, B. Fowler, J. Yang, H. Li, M. L. Steigerwald, C. Nuckolls and L. Venkataraman, *Nat. Commun.*, 2019, **10**, 4482.
56 H. Chen, H. Zheng, C. Hu, K. Cai, Y. Jiao, L. Zhang, F. Jiang, I. Roy, Y. Qiu, D. Shen, Y. Feng, F. M. Alsubaie, H. Guo, W. Hong and J. F. Stoddart, *Matter*, 2020, **2**, 378–389.
57 H. Chen, F. Jiang, C. Hu, Y. Jiao, S. Chen, Y. Qiu, P. Zhou, L. Zhang, K. Cai, B. Song, X. Y. Chen, X. Zhao, M. R. Wasielewski, H. Guo, W. Hong and J. F. Stoddart, *J. Am. Chem. Soc.*, 2021, **143**, 8476–8487.
58 M. Huang, Q. Zhou, F. Liang, L. Yu, B. Xiao, Y. Li, M. Zhang, Y. Chen, J. He, S. Xiao and S. Chang, *Nano Lett.*, 2021, **21**, 5409–5414.
59 C. Yang, L. Zhang, C. Lu, S. Zhou, X. Li, Y. Li, Y. Yang, Y. Li, Z. Liu, J. Yang, K. N. Houk, F. Mo and X. Guo, *Nat. Nanotechnol.*, 2021, **16**, 1214–1223.
60 C. Gu, C. Hu, Y. Wei, D. Lin, C. Jia, M. Li, D. Su, J. Guan, A. Xia, L. Xie, A. Nitzan, H. Guo and X. Guo, *Nano Lett.*, 2018, **18**, 4156–4162.
61 J. H. Tang, Y. Li, Q. Wu, Z. Wang, S. Hou, K. Tang, Y. Sun, H. Wang, H. Wang, C. Lu, X. Wang, X. Li, D. Wang, J. Yao, C. J. Lambert, N. Tao, Y. W. Zhong and P. J. Stang, *Nat. Commun.*, 2019, **10**, 4599.
62 W. Zhang, S. Gan, A. Vezzoli, R. J. Davidson, D. C. Milan, K. V. Luzyanin, S. J. Higgins, R. J. Nichols, A. Beeby, P. J. Low, B. Li and L. Niu, *ACS Nano*, 2016, **10**, 5212–5220.
63 H. Wen, W. Li, J. Chen, G. He, L. Li, M. A. Olson, A. C.-H. Sue, J. F. Stoddart and X. Guo, *Sci. Adv.*, 2016, **2**, e1601113.
64 C. Zhou, X. Li, H. Masai, Z. Liu, Y. Lin, T. Tamaki, J. Terao, J. Yang and X. Guo, *Small Methods*, 2019, **3**, 1900464.
65 G. C. Solomon, D. Q. Andrews, R. H. Goldsmith, T. Hansen, M. R. Wasielewski, R. P. Van Duyne and M. A. Ratner, *J. Am. Chem. Soc.*, 2008, **130**, 17301–17308.
66 C. M. Guédon, H. Valkenier, T. Markussen, K. S. Thygesen, J. C. Hummelen and S. J. van der Molen, *Nat. Nanotechnol.*, 2012, **7**, 305–309.
67 K. G. L. Pedersen, M. Strange, M. Leijnse, P. Hedegård, G. C. Solomon and J. Paaske, *Phys. Rev. B: Condens. Matter Mater. Phys.*, 2014, **90**, 125413.
68 C. J. Lambert, *Chem. Soc. Rev.*, 2015, **44**, 875–888.
69 M. H. Garner, H. Li, Y. Chen, T. A. Su, Z. Shangguan, D. W. Paley, T. Liu, F. Ng, H. Li, S. Xiao, C. Nuckolls, L. Venkataraman and G. C. Solomon, *Nature*, 2018, **558**, 415–419.
70 M. Magoga and C. Joachim, *Phys. Rev. B: Condens. Matter Mater. Phys.*, 1999, **59**, 16011–16021.
71 Z. Chen, L. Chen, G. Li, Y. Chen, C. Tang, L. Zhang, J. Liu, L. Chen, Y. Yang, J. Shi, J. Liu, H. Xia and W. Hong, *Cell Rep. Phys. Sci.*, 2021, **2**, 100329.
72 S. Gunasekaran, J. E. Greenwald and L. Venkataraman, *Nano Lett.*, 2020, **20**, 2843–2848.

73 G. C. Solomon, C. Herrmann, T. Hansen, V. Mujica and M. A. Ratner, *Nat. Chem.*, 2010, **2**, 223–228.
74 T. Markussen, R. Stadler and K. S. Thygesen, *Nano Lett.*, 2010, **10**, 4260–4265.
75 D. Fracasso, H. Valkenier, J. C. Hummelen, G. C. Solomon and R. C. Chiechi, *J. Am. Chem. Soc.*, 2011, **133**, 9556–9563.
76 J. E. Greenwald, J. Cameron, N. J. Findlay, T. Fu, S. Gunasekaran, P. J. Skabara and L. Venkataraman, *Nat. Nanotechnol.*, 2021, **16**, 313–317.
77 M. Camarasa-Gómez, D. Hernangómez-Pérez, M. S. Inkpen, G. Lovat, E.-D. Fung, X. Roy, L. Venkataraman and F. Evers, *Nano Lett.*, 2020, **20**, 6381–6386.
78 J. Bai, A. Daaoub, S. Sangtarash, X. Li, Y. Tang, Q. Zou, H. Sadeghi, S. Liu, X. Huang, Z. Tan, J. Liu, Y. Yang, J. Shi, G. Mészáros, W. Chen, C. Lambert and W. Hong, *Nat. Mater.*, 2019, **18**, 364–369.
79 Y. Li, M. Buerkle, G. Li, A. Rostamian, H. Wang, Z. Wang, D. R. Bowler, T. Miyazaki, L. Xiang, Y. Asai, G. Zhou and N. Tao, *Nat. Mater.*, 2019, **18**, 357–364.
80 L. Wang, Z. Zhao, D. B. Shinde, Z. Lai and D. Wang, *Chem. Commun.*, 2021, **57**, 667–670.
81 K. Wang, A. Vezzoli, I. M. Grace, M. McLaughlin, R. J. Nichols, B. Xu, C. J. Lambert and S. J. Higgins, *Chem. Sci.*, 2019, **10**, 2396–2403.
82 C. Tang, L. Huang, S. Sangtarash, M. Noori, H. Sadeghi, H. Xia and W. Hong, *J. Am. Chem. Soc.*, 2021, **143**, 9385–9392.
83 X. Li, Z. Tan, X. Huang, J. Bai, J. Liu and W. Hong, *J. Mater. Chem. C*, 2019, **7**, 12790–12808.
84 S. V. Aradhya, J. S. Meisner, M. Krikorian, S. Ahn, R. Parameswaran, M. L. Steigerwald, C. Nuckolls and L. Venkataraman, *Nano Lett.*, 2012, **12**, 1643–1647.
85 D. Q. Andrews, G. C. Solomon, R. P. Van Duyne and M. A. Ratner, *J. Am. Chem. Soc.*, 2008, **130**, 17309–17319.
86 M. H. Garner, H. Li, Y. Chen, T. A. Su, Z. Shangguan, D. W. Paley, T. Liu, F. Ng, H. Li, S. Xiao, C. Nuckolls, L. Venkataraman and G. C. Solomon, *Nature*, 2018, **558**, 416–419.
87 L. Rincón-García, C. Evangeli, G. Rubio-Bollinger and N. Agraït, *Chem. Soc. Rev.*, 2016, **45**, 4285–4306.
88 L. Cui, R. Miao, C. Jiang, E. Meyhofer and P. Reddy, *J. Chem. Phys.*, 2017, **146**, 092201.
89 K. Wang, E. Meyhofer and P. Reddy, *Adv. Funct. Mater.*, 2020, **30**, 1904534.
90 Y.-J. Zeng, D. Wu, X.-H. Cao, W.-X. Zhou, L.-M. Tang and K.-Q. Chen, *Adv. Funct. Mater.*, 2020, **30**, 1903873.
91 J. P. Bergfield, M. A. Solis and C. A. Stafford, *ACS Nano*, 2010, **4**, 5314–5320.
92 D. Ghosh, P. Parida and S. K. Pati, *Appl. Phys. Lett.*, 2015, **106**, 193105.
93 D. Z. Manrique, Q. Al-Galiby, W. Hong and C. J. Lambert, *Nano Lett.*, 2016, **16**, 1308–1316.
94 M. Strange, J. S. Seldenthuis, C. J. O. Verzijl, J. M. Thijssen and G. C. Solomon, *J. Chem. Phys.*, 2015, **142**, 084703.
95 R.-Q. Wang, L. Sheng, R. Shen, B. Wang and D. Y. Xing, *Phys. Rev. Lett.*, 2010, **105**, 057202.
96 P. Reddy, S.-Y. Jang, R. A. Segalman and A. Majumdar, *Science*, 2007, **315**, 1568–1571.
97 J. R. Widawsky, P. Darancet, J. B. Neaton and L. Venkataraman, *Nano Lett.*, 2012, **12**, 354–358.
98 W. B. Chang, C.-K. Mai, M. Kotiuga, J. B. Neaton, G. C. Bazan and R. A. Segalman, *Chem. Mater.*, 2014, **26**, 7229–7235.
99 G. Yzambart, L. Rincón-García, A. A. Al-Jobory, A. K. Ismael, G. Rubio-Bollinger, C. J. Lambert, N. Agraït and M. R. Bryce, *J. Phys. Chem. C*, 2018, **122**, 27198–27204.
100 M. Naher, D. C. Milan, O. A. Al-Owaedi, I. J. Planje, S. Bock, J. Hurtado-Gallego, P. Bastante, Z. M. Abd Dawood, L. Rincón-García, G. Rubio-Bollinger, S. J. Higgins, N. Agraït, C. J. Lambert, R. J. Nichols and P. J. Low, *J. Am. Chem. Soc.*, 2021, **143**, 3817–3829.
101 P. Gehring, J. K. Sowa, C. Hsu, J. de Bruijckere, M. van der Star, J. J. Le Roy, L. Bogani, E. M. Gauger and H. S. J. van der Zant, *Nat. Nanotechnol.*, 2021, **16**, 426–430.
102 R. Miao, H. Xu, M. Skripnik, L. Cui, K. Wang, K. G. L. Pedersen, M. Leijnse, F. Pauly, K. Wärnmark, E. Meyhofer, P. Reddy and H. Linke, *Nano Lett.*, 2018, **18**, 5666–5672.
103 L. Cui, R. Miao, K. Wang, D. Thompson, L. A. Zotti, J. C. Cuevas, E. Meyhofer and P. Reddy, *Nat. Nanotechnol.*, 2018, **13**, 122–127.
104 D. Segal, A. Nitzan and P. Hänggi, *J. Chem. Phys.*, 2003, **119**, 6840–6855.
105 Z. Wang, J. A. Carter, A. Lagutchev, Y. K. Koh, N.-H. Seong, D. G. Cahill and D. D. Dlott, *Science*, 2007, **317**, 787–790.
106 W. Lee, K. Kim, W. Jeong, L. A. Zotti, F. Pauly, J. C. Cuevas and P. Reddy, *Nature*, 2013, **498**, 209–212.
107 L. Cui, W. Jeong, S. Hur, M. Matt, J. C. Klöckner, F. Pauly, P. Nielaba, J. C. Cuevas, E. Meyhofer and P. Reddy, *Science*, 2017, **355**, 1192–1195.
108 L. Cui, S. Hur, Z. A. Akbar, J. C. Klöckner, W. Jeong, F. Pauly, S.-Y. Jang, P. Reddy and E. Meyhofer, *Nature*, 2019, **572**, 628–633.
109 N. Mosso, H. Sadeghi, A. Gemma, S. Sangtarash, U. Drechsler, C. Lambert and B. Gotsmann, *Nano Lett.*, 2019, **19**, 7614–7622.
110 R. Naaman and D. H. Waldeck, *Annu. Rev. Phys. Chem.*, 2015, **66**, 263–281.
111 R. Naaman, Y. Paltiel and D. H. Waldeck, *Nat. Rev. Chem.*, 2019, **3**, 250–260.
112 R. Naaman, Y. Paltiel and D. H. Waldeck, *J. Phys. Chem. Lett.*, 2020, **11**, 3660–3666.
113 S. Alwan and Y. Dubi, *J. Am. Chem. Soc.*, 2021, **143**, 14235–14241.
114 B. Verlhac, N. Bachellier, L. Garnier, M. Ormaza, P. Abufager, R. Robles, M.-L. Bocquet, M. Ternes, N. Lorente and L. Limot, *Science*, 2019, **366**, 623–627.
115 A. N. Pal, D. Li, S. Sarkar, S. Chakrabarti, A. Vilan, L. Kronik, A. Smogunov and O. Tal, *Nat. Commun.*, 2019, **10**, 5565.
116 J. de Bruijckere, P. Gehring, M. Palacios-Corella, M. Clemente-León, E. Coronado, J. Paaske, P. Hedegård and H. S. J. van der Zant, *Phys. Rev. Lett.*, 2019, **122**, 197701.
117 A. K. Mitchell, K. G. L. Pedersen, P. Hedegård and J. Paaske, *Nat. Commun.*, 2017, **8**, 15210.

118 G. Ke, C. Duan, F. Huang and X. Guo, *InfoMat*, 2020, **2**, 92–112.
119 A. C. Aragonès, D. Aravena, J. I. Cerdá, Z. Acís-Castillo, H. Li, J. A. Real, F. Sanz, J. Hihath, E. Ruiz and I. Díez-Pérez, *Nano Lett.*, 2016, **16**, 218–226.
120 B. W. Heinrich, C. Ehlert, N. Hatter, L. Braun, C. Lotze, P. Saalfrank and K. J. Franke, *ACS Nano*, 2018, **12**, 3172–3177.
121 S. Wagner, F. Kisslinger, S. Ballmann, F. Schramm, R. Chandrasekar, T. Bodenstein, O. Fuhr, D. Secker, K. Fink, M. Ruben and H. B. Weber, *Nat. Nanotechnol.*, 2013, **8**, 575–579.
122 K. Yang, H. Chen, T. Pope, Y. Hu, L. Liu, D. Wang, L. Tao, W. Xiao, X. Fei, Y.-Y. Zhang, H.-G. Luo, S. Du, T. Xiang, W. A. Hofer and H.-J. Gao, *Nat. Commun.*, 2019, **10**, 3599.
123 T. Konishi, M. Kiguchi, M. Takase, F. Nagasawa, H. Nabika, K. Ikeda, K. Uosaki, K. Ueno, H. Misawa and K. Murakoshi, *J. Am. Chem. Soc.*, 2013, **135**, 1009–1014.
124 C. Guo, X. Chen, S.-Y. Ding, D. Mayer, Q. Wang, Z. Zhao, L. Ni, H. Liu, T. Lee, B. Xu and D. Xiang, *ACS Nano*, 2018, **12**, 11229–11235.
125 H. Jeong, H. B. Li, L. Domulevicz and J. Hihath, *Adv. Funct. Mater.*, 2020, **30**, 2000615.
126 H. Jeong, L. K. Domulevicz and J. Hihath, *J. Microelectromechanical Syst.*, 2021, **30**, 126–136.
127 Z. Yu, Y.-X. Xu, J.-Q. Su, P. M. Radjenovic, Y.-H. Wang, J.-F. Zheng, B. Teng, Y. Shao, X.-S. Zhou and J.-F. Li, *Angew. Chem., Int. Ed.*, 2021, **60**, 15452–15458.